Preface

This is the third and final volume in a series of Lecture Notes based on the highly successful Euro Summer School on Exotic Beams that has been running yearly since 1993 (apart from 1999) and is planned to continue to do so. It is the aim of the series to provide an introduction to Radioactive Ion Beam (RIB) physics at the level of graduate students and young postdocs starting out in the field. Each volume contains lectures covering a range of topics from nuclear theory to experiment to applications.

Our understanding of atomic nuclei has undergone a major re-orientation over the past two decades and seen the emergence of an exciting field of research: the study of 'exotic' nuclei. The availability of energetic beams of short-lived nuclei, referred to as 'radioactive ion beams' (RIBs), has opened the way to the study of the structure and dynamics of thousands of nuclear species never before observed in the laboratory. This field has now become one of the most important and fast-moving in physics worldwide. And it is fair to say that Europe leads the way with a number of large international projects starting up in the next few years, such as the FAIR facility at GSI in Germany. From a broader perspective, one must also highlight just how widely RIB physics impacts on other areas, from energy and the environment to medicine and materials science. There is little doubt that RIB physics has transformed not only nuclear physics itself but many other areas of science and technology too, and will continue to do so in the years to come.

While the field of RIB physics is linked mainly to the study of nuclear structure under extreme conditions of isospin, mass, spin and temperature, it also addresses problems in nuclear astrophysics, solid-state physics and the study of fundamental interactions. Furthermore, important applications and spin-offs also originate from this basic research. The development of new production, acceleration and ion storing techniques and the construction of new detectors adapted to work in the special environment of energetic radioactive beams is also an important part of the science. And, due to the fact that one is not limited anymore to the proton/neutron ratio of stable-isotope beams, virtually the whole chart of the nuclei opens up for research, so theoretical models can be tested and verified all the way up to the limits of nuclear existence: the proton and neutron 'drip lines'.

The beams of rare and 'exotic' nuclei being produced are via two complementary techniques: in-flight separation and post-acceleration of low-energy radioactive beams. Both methods have been developed in a number of European Large Scale Facilities such as ISOLDE (CERN, Switzerland), GANIL (Caen, France), GSI (Darmstadt, Germany), the Accelerator Laboratory of the University of Jyväskylä (Finland), INFN Laboratori Nazionali di Legnaro (Italy) and the Cyclotron Research Centre (Louvain-la-Neuve, Belgium). Indeed, so important is the continued running and success of the School that a number of these European facilities have committed to providing financial support over the coming years.

While the field of RIB physics is linked mainly to the study of nuclear structure under extreme conditions of isospin, mass, spin and temperature, it also addresses problems in nuclear astrophysics, solid-state physics and the study of fundamental interactions. Furthermore, important applications and spin-offs also originate from this basic research. The development of new production, acceleration and ion storing techniques and the construction of new detectors adapted to work in the special environment of energetic radioactive beams is also an important part of the science. And, due to the fact that one is not limited anymore to the proton/neutron ratio of stable beams, virtually the whole chart of the nuclei opens up for research, so theoretical models can be tested and verified all the way up to the limits of nuclear existence: the proton and neutron 'drip lines'.

Volumes I and II of this series have proved to be highly successful and popular with many researchers reaching for it for information or providing it for their PhD students as an introduction to a particular topic. They are now even available to download from the Euro School Website (http://www.euroschoolonexoticbeams.be/eb/pages/lecture_notes). We stress that the contributions in these volumes are not review articles and so are not meant to contain all the latest results or to provide an exhaustive coverage of the field but are written instead in the pedagogical style of graduate lectures and thus have a reasonably long 'shelf life'. As with the first two volumes, the contributions here are by leading scientists in the field who have lectured at the School. They were chosen by the editors to provide a range of topics within the field and will have updated their material delivered at the School (sometimes several years ago) to incorporate recent advances and results.

Finally, we wish to thank the lectures who have contributed to this volume for their hard work and diligence, and indeed for their patience, at a time when everyone finds it difficult to find the time to lay out their subject in such a careful, thorough and readable style. We also wish to thank Dr. Chris Caron and his colleagues at Springer-Verlag for their help, fruitful collaboration and continued support on this project.

Guildford, UK, *J. Al-Khalili*
Darmstadt, Germany *E. Roeckl*

Testing the Structure of Exotic Nuclei via Coulomb Excitation of Radioactive Ion Beams at Intermediate Energies

T. Glasmacher

Department of Physics & Astronomy and National Superconducting Cyclotron Laboratory, Michigan State University, East Lansing, MI 48824, USA

Abstract With the advent of accelerator facilities dedicated to the production of radioactive nuclei, experimenters had to develop new, efficient techniques that can measure observables with the available beam rates. In-flight separated beams offer large luminosity gains through the use of thick secondary targets when combined with the detection of γ-rays to indicate inelastic scattering. Here we review the status of Coulomb excitation at intermediate energies, a technique that allows for the measurement of transition rates in atomic nuclei with beam rates of a few particles per second.

1 Introduction

Both experimental and theoretical nuclear scientists study atomic nuclei in the quest for predictive theoretical descriptions that explain the properties of all nuclei. Progress is made through the unremitting collaboration between theorists and experimentalists – the confrontation of testable hypotheses with precise observables measured under well-controlled conditions [1, 2]. Advances have accelerated in the past decade with the availability of accelerator facilities dedicated to the production of radioactive ions [3].

These facilities make available to experimenters the radioactive atomic nuclei that differ significantly in their properties (e.g., binding energy or proton–to–neutron ratio or radius) from stable nuclei. This in turn enables experiments to test hypotheses with atomic nuclei specifically chosen such that the predicted effect on observables may be most pronounced. Nuclear spectroscopy experiments are typically limited by background, which obscures the signals sought. Being able to work with radioactive atomic nuclei in reactions that yield the largest effect on predicted observables is thus a major advance. This advance, however, comes at a cost and with a major paradigm shift. New experimental techniques need to be developed and their efficacy established to study beams of radioactive nuclei. It is and, impractical indeed, almost always impossible to produce targets made of radioactive nuclei, most of which decay

Glasmacher, T.: *Testing the Structure of Exotic Nuclei via Coulomb Excitation of Radioactive Ion Beams at Intermediate Energies*. Lect. Notes Phys. **764**, 27–55 (2009)
DOI 10.1007/978-3-540-85839-3_2

in fractions of a second. The new paradigm in experiments with radioactive beams is that *an experiment's discovery potential is limited by the available beam rate* and nature's cross section, which we desire to measure. With stable beams, beam rate is often not a major concern, rather the cross section to be measured limits the discovery potential of experiments (neglecting at this point practical considerations, such as detectors and other necessities, which apply equally to experiments with radioactive beams). Moles of stable atoms naturally occurring on earth can be ionized during an experiment in efficient ion sources via atomic processes with cross sections which are large compared to those for nuclear processes. In radioactive beam experiments, on the other hand, each single beam particle needs to be made in a nuclear reaction before it can become available for experiments.

For a radioactive ion beam facility with a driver accelerator of given power and production mechanism, the production rate for radioactive ions drops precipitously with each nucleon further away from the valley of stability, often by more than an order of magnitude for each nucleon further away. This observation motivates a corollary to the new paradigm: *Certain observables from reactions with radioactive nuclei cannot be measured, unless an experimental technique exists that can make a meaningful measurement of the observable compatible with the production rate of the radioactive nucleus.* Given today's economics of nuclear science experiments at radioactive beam accelerator facilities (hourly operations costs are of the order of several thousand Euros) prolonging experiments by orders of magnitude is generally not a viable option. Facility upgrades to increase driver power and thus production rate by orders of magnitude can cost tens or hundreds of million Euros. This corollary has thus motivated experimentalists to devise techniques which make the most efficient use of each radioactive atom. For a given observable, the technique which can operate with the lowest beam rate will have furthest scientific reach. In other words, for the most exotic radioactive beams the question of which technique to choose is moot. Instead, it is a question of whether a technique exists at all.

In this chapter I discuss one such technique, namely Coulomb excitation of radioactive ion beams at intermediate energies with γ-ray detection. This technique allows the measurement of Coulomb excitation cross sections between specified initial and final states in atomic nuclei with beam rates of a few particles/s. From the Coulomb excitation cross sections the absolute values of transition matrix elements between the states can be deduced. These latter quantum mechanical observables are calculable in the framework of nuclear theories and can confront measured values.

1.1 Brief History of Coulomb Excitation of Radioactive Beams

Coulomb excitation is one of the oldest [4–6] and best-established experimental probes in nuclear science. The reaction mechanism between a projectile and target interacting electromagnetically is well-known and was used extensively to study electromagnetic transition strengths with stable beams and

targets starting in the 1950s [7, 8]. Such experiments were typically performed at beam energies below the Coulomb barrier to allow sufficient physical separation between the projectile and target nuclei to exclude possible nuclear contributions to the excitation mechanism.

The first Coulomb excitation experiment with a radioactive beam was published in 1991 [9]. The excited state at $E_x = 0.98\,\mathrm{MeV}$ in the neutron-rich radioactive nucleus ^{8}Li was populated by scattering a ^{8}Li beam off a $1.1\,\mathrm{mg/cm^2}$ $^{\mathrm{nat}}$Ni target at a beam energy of 14.6 MeV. The beam was produced in the transfer reaction ^{9}Be(^{7}Li,^{8}Li)^{8}Be at a rate of 10^5–10^7/s and separated in a superconducting solenoid magnet [10, 11] at the University of Notre Dame. Excited ^{8}Li nuclei were detected in a position-sensitive silicon ΔE–E telescope with an energy uncertainty of 400–500 keV, partially due to the beam energy uncertainty.

An alternative approach to detecting scattered particles is the detection of γ-rays to indicate the de-excitation of a bound excited state. This approach yields better energy resolution compared to particle detection, but it can also mean a loss in count rate due to the limited efficiency single germanium detectors. In Chap. 6, we will discuss how this loss in efficiency will be overcome with new detectors towards the end of this decade, almost 20 years after the publication of the first Coulomb excitation experiment with a radioactive beam and γ-ray detection in 1992 [12]. In this first experiment a beam of ^{76}Kr with an energy of 237 MeV and a rate of about 10^6/s was produced in the ^{9}Be(^{70}Ge,3n) reaction at the JAERI tandem accelerator. The ^{76}Kr beam was Coulomb excited through scattering off an enriched ^{208}Pb target of $2.0\,\mathrm{mg/cm^2}$ thickness and deexcitation γ-rays were detected in four germanium detectors. The observed γ-ray yield corresponding to the $2^+ \rightarrow$ g.s. transition in ^{76}Kr agreed with the yield expected from the known $B(E2; 0^+ \rightarrow 2^+)$ value. While this early experiment did not have a high-purity radioactive ion beam available as is now common at dedicated radioactive ion beam facilities, it did demonstrate that Coulomb-excitation cross sections of radioactive beams at below-barrier energies can be measured reliably from γ-ray yields in inverse kinematics. Such studies are now routinely performed at the Holifield Radioactive Ion Beam Facility at Oak Ridge National Laboratory [13–15], at REX-Isolde at CERN [16–19] and are planned in the near future at the ISAC facility at TRIUMF. At these three ISOL facilities radioactive ion beams are produced by the isotope separation on-line (ISOL) technique [20] and reaccelerated to energies below the Coulomb barrier. Radioactive beams produced via the ISOL technique can be very intense and have beam qualities akin to those encountered at stable beam facilities. Beam developments are chemistry-dependent and need thus to be optimized for each element. Refractory elements cannot be produced by the ISOL method. The low-beam energy ensures the absence of nuclear contributions to the excitation process in scattering experiments and requires the use of thin targets with thicknesses of the order of $1\,\mathrm{mg/cm^2}$. This target thickness together with typical Coulomb excitation cross sections necessitates beam rates in excess of 10^3–10^4/s to achieve typical count rates.

1.2 In-Beam γ-ray Spectroscopy Experiments with Fast Beams and Thick Targets

Intermediate-energy Coulomb excitation employs radioactive beams at energies of 30–300 MeV/nucleon ($v \approx 0.25$–$0.65\,c$) which are separated in-flight by physical means following the fragmentation or fission of a heavy-ion beam on a production target. This approach is complementary to the ISOL technique. In-flight beam developments are fast, chemistry-independent, and applicable to all species. However, with current heavy-ion drivers beam rates are lower for the elements best made via the ISOL technique. ISOL beams also have lower emittance than in-flight separated beams, whose momentum spread is determined by the fragment separator to less than a few percent. If required, the fragment momentum can be determined event-by-event through measurement of each beam particle's position at dispersive images as long as beam rates are compatible with the capabilities of a tracking detector. Cocktails of different isotopes with similar rigidities can be made available in one experiment with each beam particle identified (in charge Z and mass A) on an event-by-event basis. The large beam velocity allows beam tracking and tagging, which can reduce background, and it provides kinematic focusing that allows the efficient detection of scattered beam particles.

Most importantly, the large beam velocity enables the use of thick secondary targets (100–1,000 times thicker than at Coulomb barrier energies) in in-beam γ-ray experiments. In such experiments the number of reactions taking place $N_{\mathrm{reactions}}$ and the number of γ-rays detected, N_γ, are related to the number of atoms per area in the secondary target N_{target}, the number of beam particles impinging onto the target N_{beam}, the detection efficiency ϵ, and the cross section σ to be determined through

$$N_{\mathrm{reactions}} = \frac{N_\gamma}{\epsilon} = \sigma \times N_{\mathrm{target}} \times N_{\mathrm{beam}} \; . \tag{1}$$

In scattering experiments with stable beams, N_{beam} is not a major concern. With the new paradigm, a beam rate that is too low renders an experiment non-feasible. In most radioactive ion beam experiments, experimenters request the maximum beam rate that the accelerator facility can provide. The use of thicker targets (at intermediate energies N_{target} increases by a factor of 100–1,000 relative to low-energy experiments) translates directly into an increase in the number of reactions $N_{\mathrm{reactions}}$ and the number of detected γ-rays. Directly addressing our corollary from above, several experimental techniques have been developed to leverage this luminosity gain with radioactive ion beams at intermediate energies. Notable amongst them are in-beam fragmentation to provide excited state energies [21, 22], single-nucleon knockout reactions [23] to measure configurations in ground state wave functions and spectroscopic factors, two-nucleon knockout reactions [24–26], single-nucleon addition reactions to measure spectroscopic factors [27], and intermediate-energy Coulomb excitation [28, 29]. With the latter technique, in-flight separated beams and

thick targets allow us to measure transition matrix elements with beam rates as low as a few particles/s.

The experimenters' task is to determine the cross section σ in Eq. (1) under well-controlled conditions, accurately, and with documented precision. Experimenters communicate their experimental result in a way that enables others to draw conclusions and to reproduce the measurements. The experimental considerations to arrive at cross sections are discussed in Sect. 2. Experimenters or theorists convert the measured cross sections into physics observables that are calculable. This will be discussed in Sect. 3. Considering that a single measurement can cost several hundreds to thousand euros, both steps must be executed with care.

2 Experimental Considerations

In intermediate-energy Coulomb excitation experiments radioactive projectiles are scattered off heavy, stable targets. The scattered projectiles are detected at small scattering angles in coincidence with γ-rays emitted from the target nucleus (which is at rest or slowly recoiling in the laboratory) and the projectile which is moving with close to beam velocity slowed down only by energy loss in the target. This process is schematically illustrated in Fig. 1.

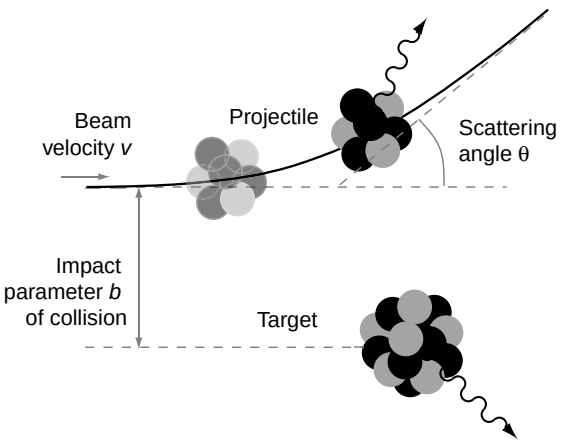

Fig. 1. Schematic illustration of the intermediate-energy Coulomb excitation process. A fast projectile ($v \approx 0.25 - 0.65$ c) impinges on a heavy target at an impact parameter b large enough to avoid nuclear contributions to the excitation process. The projectile and target can excite each other as they pass through each other's electric fields. If the excitation is to a bound excited state with sufficiently short lifetime, a γ-ray is emitted in close proximity to the target and can be detected by γ-ray detectors surrounding the target in coincidence with the scattered beam particle

The success of the measurement (an accurate cross section with defined precision) depends critically on the experimental realization of this concept. Experimenters must implement all assumptions which may be implicit in the schematic and must actively control all external circumstances which can influence the result of the measurement. Students develop these skills by working alongside experienced practitioners in the field and by learning from their peers. These time-honored methods serve experimental nuclear science well. However, it takes about two decades to gain the necessary experience and, with experiments becoming increasingly costly, the old nuclear science model to simply redo an experiment when it has failed may have outlived its timeliness. Novices learn faster and experimental success increases when they work alongside experienced practitioners and if all implicit assumptions and all external circumstances that can affect the experimental outcome are made explicit so that they can be addressed in a considered fashion.[1]

In the following, we closely examine some experimental considerations encountered in intermediate-energy Coulomb excitation experiments. While Eq. (1) does not specify a reaction, the experimenter must implement a specific reaction in the experiment.

2.1 Measuring Coulomb Excitation Cross Sections with Deexcitation γ-rays

The Coulomb excitation cross sections to excite specific states depend for a given projectile and target strongly on the incident beam energy. Figure 2 illustrates for the case of ^{40}S incident on a gold target, that low-lying collective

[1] "Considered fashion" means that the effort (or cost) expended to control a possible influence on the experimental outcome be commensurate with the benefit (or worth) derived from controlling the influence. An example may illustrate this: An in-flight separated beam has a momentum spread of 1%. In an intermediate-energy Coulomb excitation experiment, the beam passes through a thick secondary target where it loses 20% of its momentum. A γ-ray can be emitted at any time while the secondary beam traverses the secondary target. The beam velocity assumed for Doppler reconstruction is taken to be that at the mid-point of the secondary target. Should a fast tracking detector be built to measure the beam momentum of the secondary beam on an event-by-event basis to an accuracy of 0.1% to improve the γ-ray resolution? To answer this question, one could study several tracking detector designs and develop cost estimates for them. Alternatively, one can first consider the possible benefit. Since the secondary target introduces a momentum uncertainty of 20%, the initial beam momentum spread is small in comparison and any improvement will yield little benefit in the quality of the data. One concludes that the worth derived by this proposed detector is close to zero. The return on investment of resources (or the value, which is defined as worth/cost) does not warrant the expense. Experienced practitioners perform such value analyses implicitly many, many times in each experiment: Should we interrupt the experiment to repair a bad detector channel? Should we take more data in this configuration or change configurations? ...

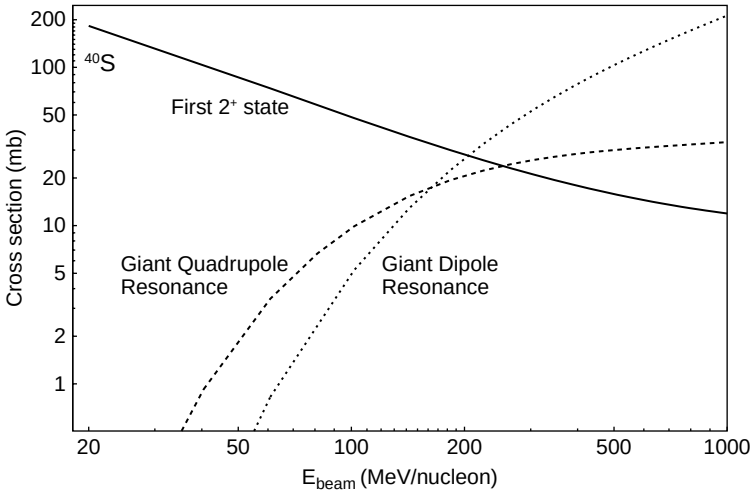

Fig. 2. Calculated cross sections for intermediate-energy Coulomb excitation at different beam energies for a ^{40}S projectile impinging on a gold target. Cross sections are shown for a low-lying collective 2^+ state, the giant quadrupole resonance, and for the giant dipole resonance

states are preferably excited at beam energies below 100–150 MeV/nucleon, while beam energies above 200–300 MeV/nucleon are better suited to excite giant resonances.

The experimenter must ensure that Coulomb excitation dominates the excitation process and that nuclear contributions are either negligible or will be appropriately accounted for. Small nuclear contributions are realized by requiring very forward projectile scattering angles $\theta_{\max}^{\text{lab}}$ in the laboratory and by ensuring that the charge and mass of the reaction product are identical to that of the projectile. This requires that the impact parameter b be larger than a minimum impact parameter $b_{\min}$ which is chosen to ensure a distance between projectile and target that avoids nuclear contributions to the excitation process. The optical model calculation in Fig. 5 illustrates the dominance of the Coulomb excitation cross section over nuclear contributions at small scattering angles.

Commonly used values for $b_{\min}$ are the sum of the projectile and target radii plus 2 fm, which exceeds the interaction radius defined by Wilcke and collaborators [32] by several tens of femtometer for heavy targets.

Since the Coulomb excitation cross section $\sigma_{i\to f}$ from an initial state $|i\rangle$ to a final state $|f\rangle$ in (1) will be determined by measuring the γ-ray yield $I_{f\to i}$ for the deexcitation $|f\rangle \to |i\rangle$ it is important to assess contributions to this yield which are not proportional to the excitation cross section. Some such possibilities are indicated in Fig. 4. The Coulomb excitation process with fast

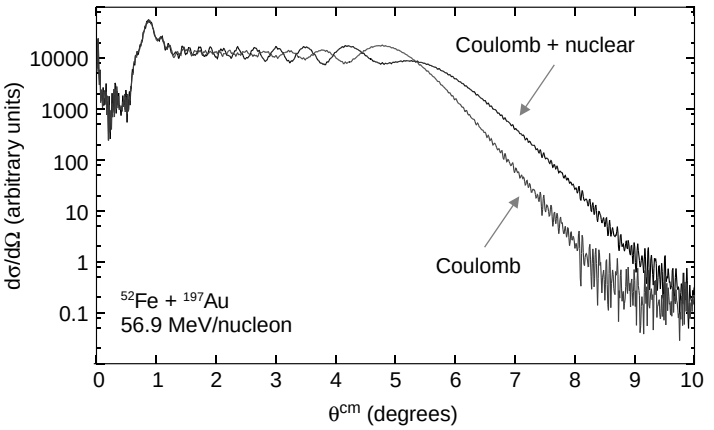

Fig. 3. Calculated excitation cross sections versus center-of-mass scattering angle $\theta^{\rm cm}$ for the reaction ^{52}Fe + ^{197}Au at 56.9 MeV/nucleon. Shown are the Coulomb excitation cross section and the Coulomb plus nuclear excitation cross sections. The Coulomb cross section dominates for small scattering angles. Optical model parameters from the ^{40}Ar + ^{208}Pb reaction at 41 MeV/nucleon [30] were used to calculate the cross sections. Figure adapted from [31] (See also Plate 5 in the Color Plate Section)

beams is generally a one-step process and multi-step excitations are highly suppressed. However, multiple low-lying states may be populated (depending on the level density and structure of the nucleus under consideration) and the

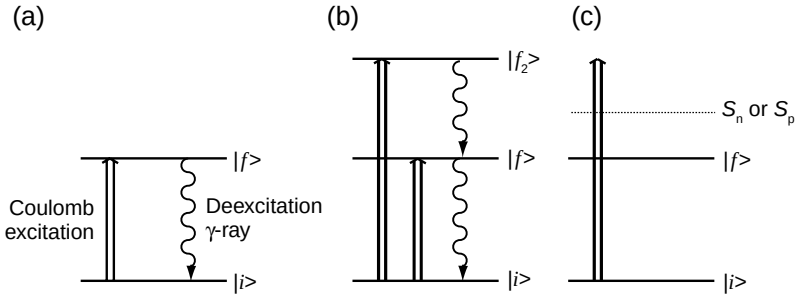

Fig. 4. Schematic illustration of measuring Coulomb excitation cross sections by counting de-excitation γ-rays from bound excited states. Panel (**a**) illustrates the desired process where a nucleus in its ground state $|i\rangle$ is Coulomb excited into a final state $|f\rangle$, which then γ-decays back to the ground state $|i\rangle$. The γ-ray yield $I_{f\to i}$ is proportional to the Coulomb excitation cross section $\sigma_{i\to f}$. If other states $|f_2\rangle$ can be Coulomb excited in the experiment they may γ-decay and feed state $|f_2\rangle$ as indicated in panel (**b**). In this case, the γ-ray yield $I_{f_2\to f}$ must be subtracted from the yield $I_{f\to i}$ to deduce the proper Coulomb excitation cross section. Excitations above the particle separation threshold may result in the breakup of the projectile. Such events are excluded from analysis since they will not be identified in the reaction product detector

possibility of feeding must be considered (see Fig. 4(b)). Electron conversion coefficients are most often negligible for the relatively fast transitions encountered with this method.

2.2 Determination of the Number of γ-rays Emitted N_γ Emitted

The γ-rays emitted from the projectile and the target are detected in the laboratory with detectors, which cover a limited solid angle and have an intrinsic γ-ray detection efficiency, which is energy-dependent. The γ-ray spectrum observed is complicated by the Doppler-shift experienced by the γ-rays emitted from the projectile. The γ-ray spectrum is also contaminated by γ-ray background that is either uncorrelated or correlated with the beam – in the latter case the correlated background γ-rays can be emitted both from in-flight sources or at rest. Experimenters determine the γ-ray yield emitted corresponding to a specific transition in the projectile or the target. This yield determination involves several steps.

The γ-ray energy spectra measured in the laboratory in coincidence with a well-identified incoming secondary beam particle and a well-identified scattered beam particle are histogrammed and energy calibrated. Random background is reduced by requiring a tight coincidence between the time at which the γ-ray is emitted and the time at which the projectile impinges on the target. With fast beams, the latter time can be determined to fractions of 1 ns on an event-by-event basis. In most applications the width of this coincidence window is determined by the time resolution of the γ-ray detectors and the discriminator used (typically 10–20 ns for germanium detectors, a few ns for many scintillators, sub-ns for BaF_2 detectors).

Photopeaks (or at high-energy escape peaks) for transitions corresponding to de-excitations in the target are visible in this spectrum. We refer to this spectrum as the laboratory energy spectrum, since γ-ray energies E_γ^{lab} detected in the laboratory are histogrammed. A second Doppler-shifted γ-ray spectrum is prepared. Histogrammed here is each γ-ray observed in the laboratory, but its energy is Doppler-shifted on an event-by-event basis to the energy at emission from the projectile, E_γ^{proj}. The two energies are related through

$$E_\gamma^{\mathrm{proj}} = E_\gamma^{\mathrm{lab}} \frac{1 - \beta_{\mathrm{emission}}^{\mathrm{lab}} \cos\theta^{\mathrm{lab}}}{\sqrt{1 - (\beta_{\mathrm{emission}}^{\mathrm{lab}})^2}}, \tag{2}$$

where θ^{lab} is the angle between the γ-ray and the scattered projectile in the laboratory and $\beta_{\mathrm{emission}}^{\mathrm{lab}}$ is the velocity of the projectile at time of γ-ray emission. Without active targets it is not practical to determine neither the velocity nor the location of γ-ray emission and thus θ^{lab} on an event-by-event basis. An emission source inside the target is generally assumed and an average velocity $\beta_{\mathrm{emission}}^{\mathrm{lab}}$ is used. This average velocity depends on the lifetime of the excited state. If this lifetime is short compared to the time in which the beam traverses the target, the beam velocity at mid-target is assumed.

If the lifetime of the excited state is long, the beam velocity after traversing the target is used. In practice, experimenters may minimize the width of the photopeak by optimizing $\beta^{\rm lab}_{\rm emission}$ between these two limits. The γ-ray yields for each transition in the projectile frame and the laboratory energy spectrum are determined. If the spectrum has few photopeaks and if the background can be well-estimated, the photopeaks can be integrated. If this is not the case, detector response functions for various energies can be simulated to reproduce source spectra measured in the laboratory. The emission function in this simulation can then be modified to simulate in-flight emission from a source with a lifetime corresponding to the state of interest (see bottom row of Fig. 5). In general, the lifetime of the state of interest is not known. If the lifetime is larger than about the time it takes the beam to traverse the target, the width of the photopeak increases since the determination of $\theta^{\rm lab}$ assumes γ-ray emission in the target. With increasing lifetime the photopeak disappears and the method becomes no longer viable. Detected, simulated γ-rays are then treated in the same fashion as measured data above to be compared to the γ-ray spectra observed in the laboratory. Starting with the highest energy photopeak, the simulated spectrum for this transition is scaled to the measured spectrum and then subtracted from the measured spectrum. This process is repeated, proceeding towards lower energies until all photopeaks are accounted for and only background remains. The scale factors for each γ-ray are proportional to their individual yields. The yields determined by either method are efficiency corrected, taking into account γ-ray absorption in the target, the intrinsic efficiency of the detector, and the solid angle covered by the detector together with the γ-ray angular distribution [33]. Care must be taken that the energy-dependent efficiency correction is applied at energy $E^{\rm lab}_\gamma$ and not at $E^{\rm proj}_\gamma$. If the γ-ray angular distribution has not been measured, it can be calculated [33] in the projectile frame and converted into the laboratory frame. These steps yield the number of γ-rays N_γ emitted from the projectiles of a specific isotope and detected in coincidence with beam particles scattered into the acceptance of the reaction product identification detector.

2.3 Beam Particles $N_{\rm beam}$ Impinging on Target

To determine the number of beam particles, $N_{\rm beam}$, in Eq. (1), the experiment must determine the number of particles of a specific species $^{\rm A}$Z incident onto the target. In other words, the number of atoms in the radioactive beam must be counted and identified before they interact with the secondary target.

At the National Superconducting Cyclotron Laboratory (NSCL), this can be accomplished by measuring the time-of-flight (and, if desired, energy loss) between two transmission detectors located about 30 m apart as illustrated in Fig. 6. The choice of detectors depends on beam rate, secondary beam purity, and composition. Generally, when beam rates are high, experimenters request secondary beams with one or only a few isotopes in the secondary beam

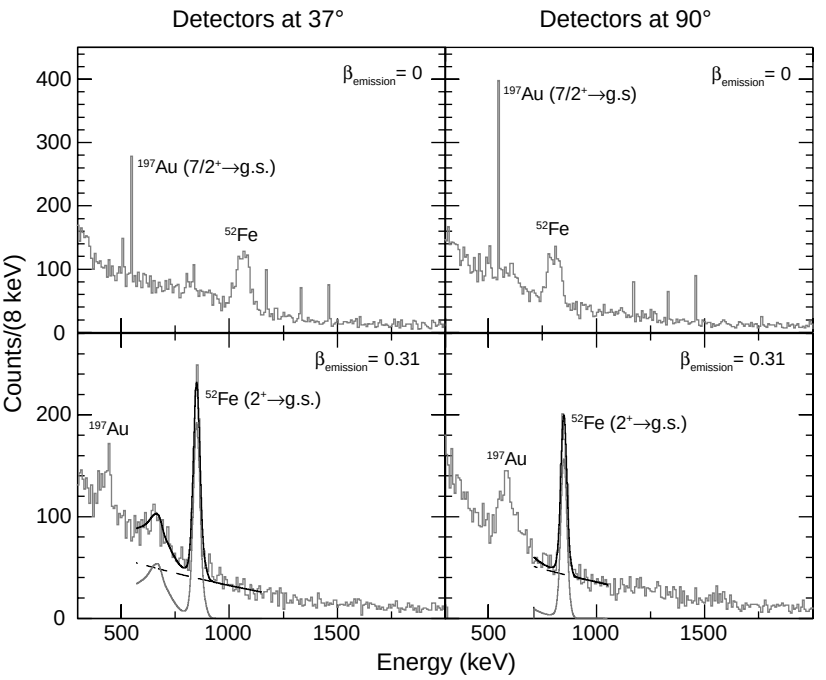

Fig. 5. Examples of laboratory energy spectra (*top row*) and projectile frame (*bottom row*) measured in the intermediate-energy Coulomb excitation of ^{52}Fe on a 257.7 mg/cm^2 (or 0.133 mm) thick ^{197}Au target. The secondary beam energy was 65.2 MeV/nucleon ($\beta = 0.356$) when impinging onto the target. The mid-target beam velocity was $\beta = 0.334$. The emission velocity for reconstruction of the Doppler-shifted γ-ray spectra was $\beta_{\rm emission} = 0.31$, which is less than the mid-target velocity. The half-life of the 849 keV first excited 2^+ state in ^{52}Fe is $T_{1/2} = 7.8(10)$ ps, which means that the projectile can travel fractions of 1 mm in one half-life. In this experiment detectors were located at two azimuthal angles with respect to the beam axis (*left and right panels*) as indicated in the *inset* of Fig. 6. The laboratory energy spectra (*top row*) show a sharp photopeak for the $7/2^+ \rightarrow$ g.s. transition at 547 keV in the ^{197}Au target, while the photopeaks corresponding to the transition in the ^{52}Fe projectile are very broad. The detectors at $\theta^{\rm lab} = 37°$ observe the 849 keV transition in ^{52}Fe at energies higher than 849 keV, since this angle corresponds to a forward angle in the center-of-mass (of the projectile–target system). Accordingly, $\theta^{\rm lab} = 90°$ corresponds to a backward angle in the center-of-mass and the energy observed in the laboratory for the 849 keV transition is less than 849 keV. In the projectile frame spectra (*bottom row*) the photopeaks of the 849 keV transition are sharp and the transitions in the gold target are broad. At 37°, the Compton edge of the photopeak is visible, while it is less pronounced at 90° where the energies detected in the laboratory are lower and the cross section for the Compton effect is thus less. Indicated as *gray solid lines* are scaled simulated response functions, which when added to the background (*dashed gray line*) reproduce the observed γ-ray spectra well. This figure was adapted from [31]

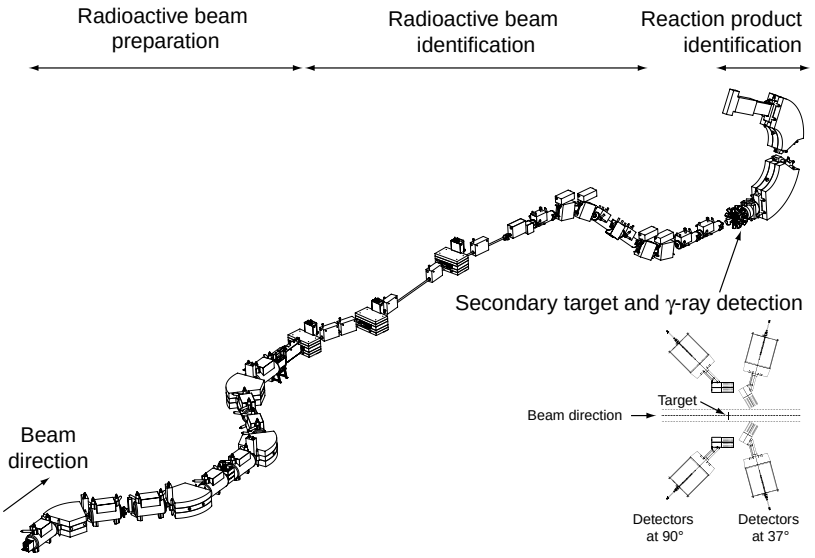

Fig. 6. Design model of the radioactive ion beam facility at NSCL. While details differ, the facilities at GANIL, GSI, and RIKEN have the same functionalities. Radioactive beams are produced by fragmentation or fission of a primary beam on the production target at the entrance to the A1900 fragment separator. The magnets in the A1900 select the isotopes of interest by rigidity ρ ($\rho = p/q$, where p is the beam particle's momentum and q its charge state). During the optimization of beam rate and purity ions are identified and stopped in detectors in the A1900 focal plane. The optimized beam is then transmitted to the secondary target through the beam transport system. A thin transmission scintillator or diamond detector located after the A1900 focal plane records a time signal for each beam particle and a second detector can be located in the intermediate image of the S800 beam analysis line. This detector can either be another timing detector or, if beam rates are low enough, a thin silicon transmission detector to measure energy loss. Located at the focal point of the S800 spectrograph [34] is the secondary target which is surrounded by γ-ray detectors. Indicated here are the 32–fold segmented high-purity germanium detectors from SeGA [35]. The S800 spectrograph identifies each scattered projectile and determines its momentum vector

cocktail in order to enhance the count rate of the primarily desired reaction channel. When only a few isotopes are in the beam cocktail, identification by time-of-flight is often sufficient to resolve the distinct masses of the isotopes. When beam rates for the isotope of interest are low, experimenters often request a number of isotopes in the beam cocktail to leverage the investment of beam time with minimal impact on data acquisition dead-time. In this latter case a thin silicon detector may replace the second timing detector and incoming beam particles may be identified by energy-loss versus time-of-flight measurements.

Experimenters carefully assess what fraction of counted and identified beam particles actually impinges onto the secondary target. While this fraction is ideally unity, transmission through additional beam transport systems after the beam identification and counting must be measured and monitored during the experiment. (At NSCL, there are 13 m of additional beam transport before the secondary target). Locating a counting detector directly adjacent to the secondary target may be advisable in certain experiments, but the possibility of it generating γ-rays must be considered carefully in intermediate-energy Coulomb excitation experiments. Special care should also be taken to ensure that the secondary target is large enough to accommodate the profile of the secondary beam and that the secondary beam does not hit the target holder. As a precaution, one wants to ensure that the energy loss in the target is different enough from all other possible beam paths, so that beam not impinging onto the target either does not get transmitted to or can be identified in the reaction product identification detector. The more general idea is to work hard to avoid possible errors, but to make them as explicit as possible should they occur. This may allow a data set to be saved through more elaborate analysis.

During the experiment certain devices must be monitored more carefully than others, depending on whether or not a failure of the particular device affects the measured cross section or not:

- A change in beam composition, a change in the beam transport system prior to beam identification, or a failure of the incoming beam identification system results in fewer incoming beam particles that are correctly identified. Since correct incoming beam identification will be a condition in the analysis, there will be fewer events, but the cross section will not be affected.
- A change in the transmission of the beam transport system after beam identification, however, can affect the cross section, since the number of beam particles impinging on the target N_{beam} is the product of the particles identified and counted and the transmission after counting.

Most radioactive ion beam facilities have control systems that can capture facility configurations and alert the experimenters of deviations during the experiment. Experimenters should double-check that all relevant optical devices are included in the captured configuration.

If the acceptance of the reaction product detector is large enough to accept the entire elastically and inelastically Coulomb scattered beam, experimenters at times approximate N_{beam} with the number of identified and scattered beam particles. This approximation relies on the Coulomb elastic scattering cross section being dominant over all others.

2.4 Number of Scattering Centers in the Target N_{target}

The number of scattering centers per unit area in the target can be calculated from the thickness d and volume density ρ of the target material when foils are used. Uniform target thickness and density are important, but can be realized relatively easily since most targets used in intermediate-energy Coulomb excitation experiments are self-supporting metal foils. Care must be taken that the target is stably and reproducibly mounted at a known angle with respect to the beam so that the effective thickness remains constant over the experiment. In addition, the position of the target along the beam axis relative to the γ-ray detectors must be known for the Doppler reconstruction of γ-rays discussed earlier.

While isotopic purity of targets is not required for Coulomb excitation of the projectile, knowledge of the isotopic composition is necessary to determine the Coulomb excitation cross section of the isotopes in the target, which provides a valuable cross check. In addition, discrete γ-rays emitted from the target appear very broadened after being Doppler shifted into the projectile frame. For this reason most experiments are performed with monoisotopic (e.g., ^{197}Au and ^{209}Bi) or isotopically enriched targets (e.g., ^{208}Pb). If the energy of the γ-ray to be measured is known or can be anticipated, secondary targets are often chosen so that the energy regions of the target and projectile γ-rays are not close to each other.

2.5 Presentation of experimental results

After the the Coulomb excitation cross section σ in Eq. (1) is determined it must be presented together with sufficient information so that others can deduce a transition rate. We discuss here the information needed and possible sources of error when converting a cross section into a transition rate.

The experimental cross section σ is measured in a particular reaction with an experimental setup, in which scattered beam particles are detected and identified in a reaction product detector, which has a particular acceptance ϵ_{RPD}. Thus

$$\sigma = \int_{\Omega} \frac{\mathrm{d}\sigma(\theta')}{\mathrm{d}\Omega'} \epsilon_{\mathrm{RPD}}(\theta', \phi') \mathrm{d}\Omega'. \tag{3}$$

Often the reaction product detector's acceptance is symmetric and uniform of the form

$$\epsilon_{\mathrm{RPD}}(\theta, \phi) = \begin{cases} 1 & \text{for } \theta < \theta_{\mathrm{max}} \\ 0 & \text{otherwise} \end{cases} . \tag{4}$$

In this case the communication of the maximum scattering angle in the laboratory $\theta^{\mathrm{lab}}_{\mathrm{max}}$ suffices to describe the solid angle over which the cross section was measured. If the reaction product detector acceptance is not uniform in ϕ or θ experimenters must communicate the acceptance as a function of θ and ϕ. Preferably, the acceptance ϵ_{RPD} is expressed as a function of θ alone (see, for

example, Fig. 2 in [36]). When deducing transition rates from cross sections, the theoretical cross section must be integrated over the same acceptance ϵ_{RPD} as was realized in the experiment. Care must also be taken to choose the proper frame of reference. Acceptances are generally given in the laboratory frame while calculations are usually performed in the center-of-mass system. The center-of-mass scattering angle θ^{cm} is related to the one in the laboratory θ^{lab} through

$$\tan\theta^{\mathrm{lab}} = \frac{\sin\theta^{\mathrm{cm}}}{\gamma(\cos\theta^{\mathrm{cm}} + \frac{\beta^{\mathrm{cm}}}{\beta^{\mathrm{proj}}})}. \tag{5}$$

Here, while β^{cm} is the center-of-mass velocity of the projectile–target system while the projectile velocity β^{proj} should be taken as the mid-target velocity of the projectile. This approximates the velocity dependence of Eq. (5) appropriately for experiments where the velocity change in the target is small relative to the velocity of the incoming beam. Thus, it is recommended that experimentalists report the mid-target velocity explicitly. The mid-target beam energy should also be reported and used as effective beam energy in theoretical calculations. Evaluating the cross section at mid-target beam energy $E_{\mathrm{beam}}(d_{\mathrm{target}}/2)$ approximates the average of the cross section $\sigma(E_{\mathrm{beam}}(x))$ over target thickness d_{target}.

3 Extraction of Transition Matrix Elements from Cross Sections

The Coulomb excitation process at energies below the Coulomb barrier has been extensively described in the literature [8, 37] and treated fully quantum-mechanically [38]. At low energies the relative motion between projectile and target follows the classical Rutherford trajectories and relativistic effects are negligible. At relativistic energies straight-line trajectories are a very good approximation. At intermediate energies, relativistic effects are still important, but straight-line trajectories can no longer be assumed and one has to consider two relativistic charged particles moving with respect to each other. This problem can be solved analytically only if the mass of one particle in the scattering process is infinite. This is schematically illustrated in Fig. 1 where the target nucleus does not recoil. Winther and Alder and Alder described the relativistic Coulomb excitation process semi-classically in 1979 [28]. To account for the recoil of the target as a first-order deviation from straight-line trajectories the impact parameter b was rescaled to

$$b \to b + \frac{\pi a}{2\gamma}, \tag{6}$$

where γ is the relativistic Lorentz factor $\gamma = 1/\sqrt{1-\beta^2}$ and a is the half-distance of closest approach in a non-relativistic head-on collision

$$a = \frac{Z_{\rm proj} Z_{\rm target} e^2}{m_0 \beta^2 c^2}. \tag{7}$$

Here, $Z_{\rm proj}$ and $Z_{\rm target}$ are the respective charges of the projectile and target and m_0 is the reduced mass of the projectile–target system. β is the beam velocity relative to the speed of light c.

Winther and Alder decompose the Coulomb excitation cross section into the sum of the allowed multipole matrix elements characteristic of the electromagnetic decay of the nuclear state $|f>$ to state $|i>$ as

$$\sigma_{i\to f} = \sum_{\pi\,\lambda} \sigma_{\pi\,\lambda}. \tag{8}$$

The individual contributions of multi-polarity λ and parity π for straight-line trajectories with impact parameters larger than a minimum impact parameter $b_{\rm min}$ are of the form

$$\sigma_{\pi\,\lambda} \approx \left(\frac{Z_p e^2}{\hbar\, c}\right)^2 \frac{\pi}{e^2\, b_{\rm min}^{2\lambda-2}} B(\pi\lambda, 0 \to \lambda) \begin{cases} (\lambda-1)^{-1} & : \quad \text{for } \lambda \geq 2 \\ 2\ln\left(b_{\rm a}/b_{\rm min}\right) & : \quad \text{for } \lambda = 1. \end{cases} \tag{9}$$

Here, $b_{\rm a}$ denotes the impact parameter at which the adiabatic cutoff of the Coulomb excitation process sets in. This occurs when the time of internal motion in the nucleus $\hbar/E_\gamma$ equals the collision time $b_{\rm a}/(\gamma\, c\, \beta)$, where E_γ is the energy of the excited state $|f>$ relative to the initial state $|i>$. Thus

$$b_{\rm a} = \frac{\gamma\, \hbar\, c\, \beta}{E_\gamma}. \tag{10}$$

Equation (10) implies that the maximum energy of final states that can be excited in collisions with impact parameter b is of the order of

$$E_\gamma^{\rm max} \approx \frac{\gamma\, \hbar\, c\, \beta}{b}. \tag{11}$$

Equation (11) illustrates why giant resonance experiments are best-performed at beam energies above 200–300 MeV/nucleon as illustrated in Fig. 2.

$b_{\rm min}$ is the minimum impact parameter realized in the experiment

$$b_{\rm min} = \frac{a}{\gamma} \cot(\Theta_{\rm max}^{cm}/2), \tag{12}$$

where theta is the maximum scattering angle $\Theta_{\rm max}^{cm}$ of the projectile in the center–of–mass system. The conversion of the maximum scattering angle into the laboratory is given in Eq. (5). The Coulomb excitation cross section $\sigma_{i\to f}$ is directly related to the reduced transition probability $B(\pi\lambda; i \to f)$ as shown in Eq. (9).

The Weizsäcker–Williams method developed in 1934 provides an alternative approach and describes the Coulomb excitation process in terms of

equivalent photon numbers [39, 40]. Coulomb excitation is understood as the absorption of virtual photons which are produced by relativistically moving charged particles. The equivalent photon number $n_{\pi\lambda}$, the number of real photons that would have the equivalent net effect on a particular transition, relates to the photo-absorption cross section $\sigma_{i\to f} \propto n_{\pi\lambda}\sigma_{abs}$. The idea underlying the Weizsäcker–Williams method had already been used in 1924 by Fermi to connect the absorption of X-rays by atoms and the energy loss due to ionization [41].

In 1984, Hoffman and Baur [42] showed that the equivalent photon method and the semi-classical approach by Alder and Winther [28] provide the same results for relativistic $E1$ Coulomb excitation cross sections [42]. At the same time Goldberg [43] extended the virtual photon method to all multipolarities [43].

Bertulani and collaborators [44, 45] performed self-contained derivations and showed that a quantum theory leads to minor modifications of the classical results [46]. A coupled channels description of intermediate-energy Coulomb excitation was developed in 2003 [47]. The interplay between relativistic retardation effects, which are included in the relativistic description of Coulomb excitation, and the correct treatment of recoil effects in the classical theory (recoil effects are only approximated through Eq. (6) in the relativistic theory) was investigated in [48].

Extending this work, Bertulani, Stuchberry, and collaborators [49] developed an exact numerical solution for the Coulomb excitation cross section and then reviewed the importance of including relativistic dynamics and the appropriate trajectories over a large range of beam energies. Cross sections to low-lying collective states at intermediate energies are dominated by collisions at large impact parameters and recoil corrections are less important than for high-energy excitation, such as giant resonances, which are dominated by collisions at small-impact parameters. For the first excited state in ^{40}S at 0.89 MeV, the difference between cross sections calculated with the exact numerical solution and semi-classically with the impact parameter rescaled (see Eq. (6)) is less than 5% above 50 MeV/nucleon [49].

The influence of nuclear excitations and the possibility of Coulomb nuclear interference need to be considered in the data analysis, especially for light nuclei and for reactions where experimenters desire to include data at larger scattering angles to increase statistics. These issues are discussed in Sect. 4 in the context of experimental results on the neutron-halo nucleus ^{11}Be.

4 Recent Experimental Results

In the past decade intermediate-energy Coulomb excitation has become a spectroscopic tool in use at all four major facilities that provide in-flight separated radioactive beams: GSI (Germany), GANIL (France), Michigan State University (USA), and RIKEN (Japan). Here we discuss two regions in the

nuclear chart, where this method has contributed to discoveries. Unexpected results can be exciting and lead to new insights, or they can be wrong and be disproven at a later time. The beauty of experimental science is that controversies always work themselves out over time.

4.1 The Neutron-Halo Nucleus ^{11}Be

^{11}Be is a loosely bound neutron-halo nucleus. Its neutron-separation energy is $S_n = 504(6)$ keV and only one bound excited state exists at 320 keV ($J^\pi = 1/2^+$). This state decays to the ground state ($J^\pi = 1/2^-$) through the fastest known dipole transition between bound states in atomic nuclei. The strong coupling between the two states was discovered in 1983 by Millener and collaborators in a lifetime measurement at Brookhaven National Laboratory which yielded a transition strength of $B(E1, 1/2^+_{\text{g.s.}} \rightarrow 1/2^-) = 0.116(12)\,\text{e}^2\text{fm}^2$ [50]. In 1995 a Coulomb excitation experiment at GANIL (of ^{11}Be on a lead target at 43 MeV/nucleon) reported a cross section that when analyzed in the semi-classical theory of Winther and Alder [28] yielded a transition strength of about 40% of the strength observed in the lifetime measurement [51]. This large discrepancy led to several studies that investigated in detail the influence of certain assumptions made in the semi-classical model.

The neutron-separation energy in ^{11}Be is small (504(6) keV) and coupling to the continuum may affect the deduced transition strength. For example, ^{11}Be after being excited into its bound excited state may be excited into the continuum in a second step. Typel and Baur studied this by extending the single-step theory to multi-step higher-order electromagnetic interactions [55]. These effects could account for a possible reduction of the $B(E1)$ strength observed in [51] to 95.5–89.9% of the value from the lifetime measurement. Similar results were observed by Bertulani and collaborators [56] in a semi-classical coupled channels approach that couples the bound states to the continuum and includes nuclear coupling effects. Only a 5% cross section reduction compared to the cross section anticipated from the lifetime transition strength could be explained and the authors conclude that "first order perturbation theory is appropriate to calculate the cross section" [56].

In the analysis according to Winther and Alder nuclear excitations are excluded in an approximate way through the introduction of a minimum impact parameter b_{min}. The standard prescription to determine b_{min} is the sum of the projectile and target nucleus plus several femtometer or the use of the interaction radius [32]. These definitions of a minimum impact parameter may not be applicable for ^{11}Be with its diffuse neutron halo. This question was investigated by Tarutina, Chamon, and Hussein [57] who multiplied the impact-parameter dependent Coulomb excitation probability by the impact-parameter dependent survival probability during integration, instead of assuming a hard cutoff b_{min}. This more accurate treatment of nuclear absorption yielded an increase in the deduced transition strength of 2% for the result in [51] and increases up to 5% for later experiments [53, 54]. While

each of these small corrections improve on the analysis with the Alder and Winther theory, they cannot individually or when combined explain the small cross section observed in [51].

In 1997, intermediate-energy heavy-ion scattering experiments at RIKEN and Michigan State University (MSU) were performed to elucidate the GANIL result. At RIKEN, Nakamura and collaborators scattered ^{11}Be off a lead target (350 mg/cm^2) at a beam energy of 63.9 MeV/nucleon and observed a large cross section of $302 \pm 8 \pm 30$ mb corresponding to a transition rate of $B(E1, 1/2^+_{\text{g.s.}} \rightarrow 1/2^-) = 0.099(10)\,\text{e}^2\text{fm}^2$. At MSU beams of ^{11}Be were scattered of ^{9}Be (195 mg/cm^2), $^{\text{nat}}$C (411 mg/cm^2), ^{197}Au (533 mg/cm^2), and ^{208}Pb (80 mg/cm^2) at mid-target beam energies of 58.4, 56.7, 57.6, and 59.4 MeV/nucleon, respectively. Excitation cross sections to the first excited state of 1.7(2)(4), 4.0(2)(5), 244(7)(24), and 304(10)(33) mb were observed, respectively. The thick gold target necessitated a correction of the observed γ-ray yield by 75% due to the strong absorption of the 320 keV photon in the target. Transition strengths extracted for the gold and lead targets were $B(E1, 1/2^+_{\text{g.s.}} \rightarrow 1/2^-) = 0.079(8)$ and $0.094(11)\,\text{e}^2\text{fm}^2$, respectively. The measurements at RIKEN and MSU were consistent with each other and the lifetime measurement, while they did not agree with the GANIL result. In addition, the small excitation cross sections on the light targets indicate that nuclear contributions are small. The effect of Coulomb-nuclear interference was investigated [58] for the case of ^{11}Be scattering in a full quantum calculation (with both nuclear and Coulomb potentials) through continuum discretized coupled channels calculations. For the light neutron-halo nucleus ^{11}Be scattering off a heavy target Coulomb nuclear interference can be both constructive or destructive and cannot be neglected even when selecting events with large impact parameters only.

In 2007 a new experiment was performed at GANIL [52] to measure the excitation cross section of ^{11}Be on ^{208}Pb at 38.6 MeV/nucleon. A cross section of 416(66) mb was observed, corresponding to a transition rate of $B(E1, 1/2^+_{\text{g.s.}} \rightarrow 1/2^-) = 0.105(12)\text{e}^2\text{fm}^2$, consistent with the measurements at RIKEN and at MSU. The deduction of the transition strength from the measured cross section in [52] was performed with the extended discretized coupled channels method, a fully quantum mechanical description of Coulomb excitation with coupling to the continuum. In contrast to the earlier theoretical analyses described earlier and the small cross sections measured on light targets, the authors find that the "excitation process involves significant contributions from nuclear, continuum, and higher-order effects".

Figure 7 summarizes the deduced transition strengths $B(E1, 1/2^+_{\text{g.s.}} \rightarrow 1/2^-)$ in ^{11}Be. The measurements on lead targets at RIKEN, MSU and the later measurement at GANIL agree well with each other and the lifetime measurement. The measurement on the gold target is consistent with the other measurements, but may suffer from an underestimation of the systematic error introduced in the 75% correction of the photon yield due to absorption in the target. The low-cross section reported in [51] cannot be reproduced.

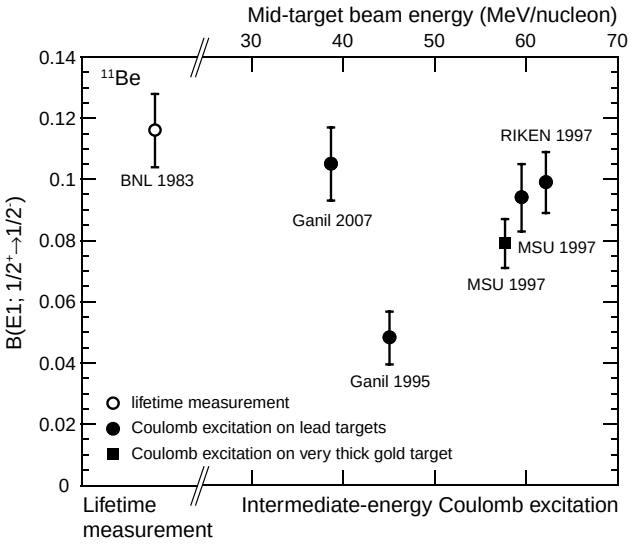

Fig. 7. Transition rates $B(E1, 1/2^+_{\text{g.s.}} \rightarrow 1/2^-)$ in ^{11}Be plotted versus beam energy. The *open circle* denotes the lifetime measurement at Brookhaven National Laboratory [50]; *solid circles* indicate experiments on relatively thin lead targets at GANIL in 2007 [52] and 1995 [51], at RIKEN in 1997 [53] and at Michigan State University (MSU) in 1997 [54]. The *solid square* denotes an experiment at MSU in 1997 [54] on a thick gold target, which required a 75% correction for photon absorption in the target

4.2 ^{30,32,34}Mg and the Island of Inversion

In 1975 Thibault and collaborators [59] found that the neutron-rich sodium isotopes are more tightly bound than expected by shell model calculations in the $\nu(sd)$ model space. Based on Hartree–Fock calculations this observation was attributed by Campi and collaborators [60] to strongly deformed ground states due to the filling of $\nu f_{7/2}$ negative parity orbitals. Shell model calculations [61] suggested that the ground state configurations of $^{30-32}$Ne, $^{31-33}$Na, and $^{32-34}$Mg are dominated by intruder configurations $\nu(sd)^{(N-2)}(f_{7/2})^2$ and form an "island of inversion" in the table of isotopes where such configurations are more energetically favorable rather than the normal $\nu(sd)^N$ configurations.

The large transition rate $B(E2, 0^+_{\text{g.s.}} \rightarrow 2^+_1) = 454(78)\,\text{e}^2\text{fm}^4$ in ^{32}Mg measured by Motobayashi and collaborators at RIKEN [36] was successfully explained by shell model calculations with $\nu(sd)^{(N-2)}(f_{7/2})^2$ configurations in the ground state and in the first excited 2^+ state supporting the idea of the island of inversion. Subsequent measurements at MSU [62, 63] and at RIKEN [64] confirmed the original result. The MSU data were also analyzed under the assumption of possible feeding into the 2^+ state via a 1,436 keV γ-ray. Such a γ-ray was observed in β-decay studies of ^{32}Na [65]. It remains an experimental questions as to whether or not this 1,436 keV γ-ray is observed

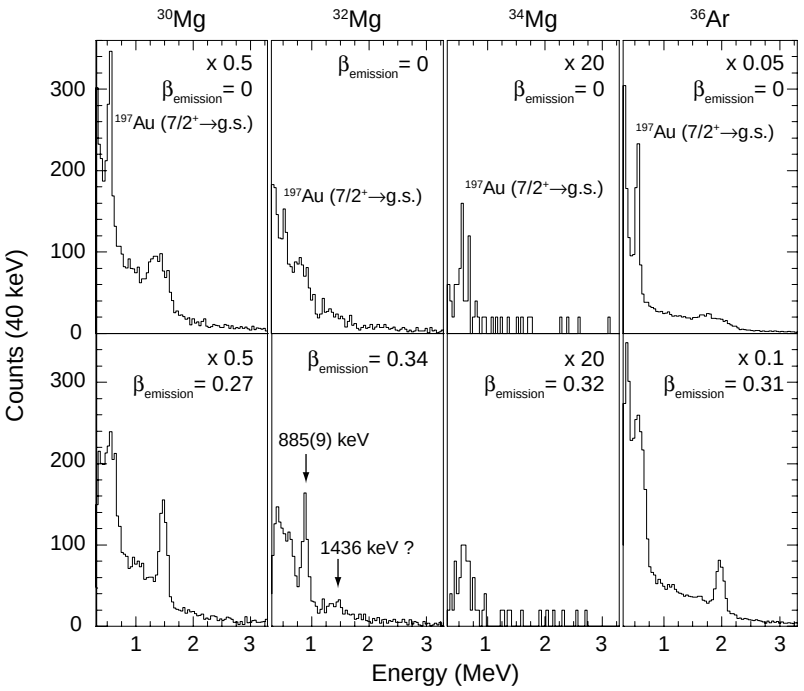

Fig. 8. Energy spectra measured in the intermediate-energy Coulomb excitation of ^{30,32,34}Mg on gold targets (518, 702, and 702 mg/cm^2 thick, respectively) at beam energies of 36.5, 57.8, and 50.6 MeV/nucleon, respectively. The γ-ray spectrum for the ^{36}Ar test case is also shown. The question as to whether or not a 1,436 keV γ-ray is visible in the ^{32}Mg spectrum remains open. Figure adapted from [62]

in intermediate-energy Coulomb excitation. Both the γ-ray spectra at MSU and RIKEN are statistics-limited and inconclusive. The spectra from [62] are shown in Fig. 8 so that the reader may assess the situation. If such a feeding transition is present, it would originate from an excited state with J^π=1^-, 1^+, or 2^+ and would reduce the cross sections and $B(E2)$ values in both the RIKEN and MSU experiments.

Transition rates measured in ^{34}Mg both at RIKEN [64] and MSU [63] agree with each other and can be understood in calculations where the ground state and the excited state are dominated by intruder configurations (Fig. 9). An intermediate-energy Coulomb excitation measurement at GANIL [66] yielded a transition rate in ^{32}Mg which is about 35% larger than the RIKEN and MSU values. The origin of this difference is currently not understood. If the GANIL value is correct and interpreted in a rotational model, it would indicate a very large charge deformation of $\beta_C = 0.61(4)$ for ^{32}Mg[66]. In the same experiment a transition rate of 435(58) e^{2}fm^4 for ^{30}Mg was deduced which is 47% larger than the MSU value of 295(26) e^{2}fm^4 [63]. The latter value

is in agreement with the recent low-energy Coulomb excitation experiment performed at REX-isolde, which found $B(E2, 0^+_{\text{g.s.}} \rightarrow 2^+_1) = 241(31)\,\text{e}^2\text{fm}^4$ in ^{30}Mg.

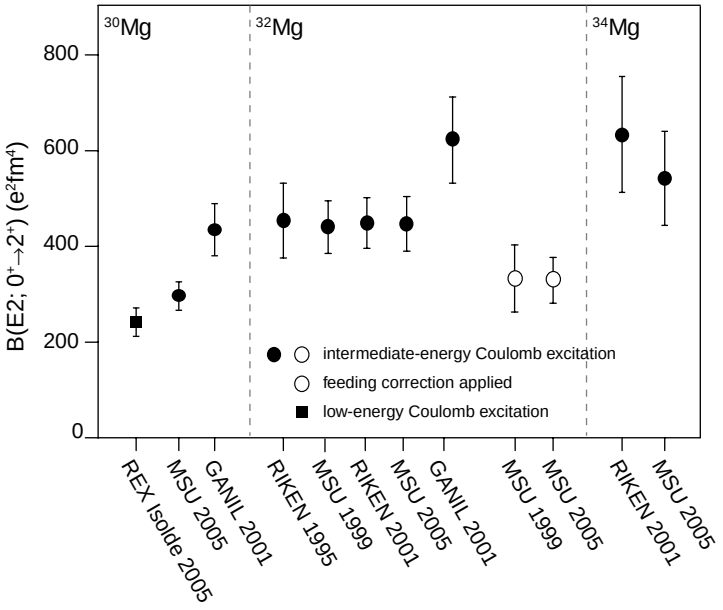

Fig. 9. Measured transition rates $B(E2, 0^+_{\text{g.s.}} \rightarrow 2^+_1)$ in ^{30,32,34}Mg. In ^{30}Mg the low-energy measurement at REX-isolde [16] agrees with the intermediate-energy measurement at MSU [63], but not with the measurement at GANIL [66]. This latter experiment also yields a larger $B(E2)$ value for ^{32}Mg, compared to the measurements at RIKEN [36, 64] and MSU [62, 63], provided no feeding correction is applied to the photon yield for the 885 keV transition. The transition rates for ^{34}Mg measured at RIKEN [64] and MSU [63] are in agreement with each other

5 Accuracy of the Technique

Whenever a new experimental technique is developed, its efficacy needs to be carefully established to avoid confusion and the unnecessary expense of effort that arises when results with questionable accuracy are published. A good way to establish the credibility of a new technique is to measure well-established observables that have been measured previously with different techniques at various laboratories. Since intermediate-energy Coulomb excitation measurements can easily measure transition rates in isotopic chains, well-known transition rates in stable isotopes have been measured in many experiments that also established new transition rates on radioactive isotopes.

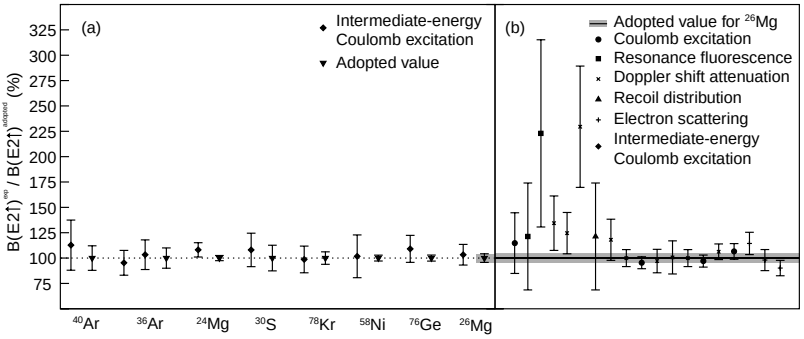

Fig. 10. Ratio of measured to adopted $B(E2; 0^+_{\text{g.s.}} \rightarrow 2^+_1)$ values for eight different stable isotopes (panel (**a**)). The transition rates plotted were measured as stable-beam test cases in intermediate-energy Coulomb excitation experiments (^{40}Ar [67],^{36}Ar [68, 69], ^{24}Mg [70],^{30}S [71],^{78}Kr [72],^{58}Ni [73], ^{76}Ge [74],^{26}Mg [63]) between 1999 and 2005. For each isotope, the transition rates are compared to the adopted values [75] for the same transition. The average difference between the measured and adopted transition rate is 6%. To put this difference into perspective, panel (**b**) compares the same ratio of measured to adopted $B(E2; 0^+_{\text{g.s.}} \rightarrow 2^+_1)$ values for ^{26}Mg. Here, the experimental values have been measured with a variety of "established" experimental probes (data taken from [75]) between 1961 and 1982. The absolute difference between the measured values and the adopted value for ^{26}Mg is 23%, while it is 3% for the intermediate-energy Coulomb excitation result [63]. This figure has been adapted from [76]

Through use of the same experimental setup and an identical analysis procedure, the measurement of these stable-beam "test cases" and comparison of the derived observables to adopted values, lends credence to newly measured observables on radioactive nuclei. Results from eight such measurements on stable isotopes are shown in Fig. 10. Of particular importance is the fact that these transition rates were measured in nuclei moving at about 30–40% of the speed of light in identical conditions to the newly measured transition rates. The comparison between the adopted and measured values then tests the complete analysis procedure. A lesser degree of certainty is provided by a comparison between the transition rate in the target (where the γ-ray was emitted at rest) and an adopted value, since the γ-ray yield from target nuclei does not undergo the kinematic reconstruction needed for γ-rays emitted from the projectile. Agreement between measured and adopted transition rates for target excitations is necessary to demonstrate the efficacy of an experiment, but it is not sufficient. Agreement between measured and adopted transition rates for excitations of the projectile is very close to sufficient.

Figure 10 shows the average difference between adopted transition rates for the stable isotopes and values measured at NSCL. The values presented here set an empirical scale for the overall accuracy of the technique. Two components contribute to the precision and accuracy of the technique. The first arises

from the experimental measurement of the cross section and was discussed in Sect. 2. The second component arises from the extraction of a transition rate from the experimental cross section and was discussed in Sect. 3. These two components are largely independent and the overall accuracy of the technique compares very favorably with other established techniques. Proper quantum calculations must be performed to account for Coulomb-nuclear interference when scattering light halo nuclei, such as ^{11}Be as discussed.

6 Outlook and Summary

In the past 10 years intermediate-energy Coulomb excitation of radioactive ions has become an established technique employed at all major radioactive beam facilities that provide in-flight separated beams worldwide. Transition rates have been measured with beam rates as low as 3 atoms/s [77]. The γ-ray detectors used in these experiments have either been scintillation detectors [78, 79] with good efficiency and moderate energy resolution or segmented high-purity germanium detectors [35, 80, 81] with good energy resolution and small photopeak efficiency (2–7% at 1,332 keV). A new concept for the efficient detection of γ-ray radiation with high-photopeak efficiency, large peak-to-background ratio, and very good position resolution is being developed. The γ-ray energy tracking array (GRETA) [82] in the United States and the advanced gamma tracking array (AGATA) [83, 84] in Europe will have more than 40% photopeak efficiency (for a single γ-ray at 1,332 keV) and will be able to determine the first interaction point of a γ-ray in the detector with an accuracy of about 2 mm (rms). The availability of such detectors will increase the sensitivity of current-day intermediate-energy Coulomb excitation experiments by more than an order of magnitude. The precision of the analysis of intermediate energy Coulomb excitation cross sections was long limited to about 5–10% secondary to the simplifying assumptions made in the semi-classical theory. With the advent of a theory that contains relativistic kinematics and dynamics and a correct treatment of the Coulomb trajectories [49], the precision of the analysis has been taken to the next level.

References

1. K. Popper, *Logik der Forschung* (Wien, 1935)
2. K.R. Popper, *The logic of scientific discovery* (Hutchinson, London, 1959)
3. R.I.S.A. Committee, (National Academies Press, Washington, 2007)
4. E. Fermi, Z. Phys. **29**, 315 (1924)
5. C.F. Weizsäcker, Z. Phys. **88**, 612 (1934)
6. E.J. Williams, Phys. Rev. **45**, 729 (1934)
7. K. Alder, A. Bohr, T. Huus, B. Mottelson, A. Winther, Rev. Mod. Phys. **28**, 432 (1956)

8. K. Alder, A. Winther, *Coulomb Excitation* (Academic Press, New York, 1966)
9. J.A. Brown, F.D. Becchetti, J.W. Jänecke, K. Ashktorab, D.A. Roberts, J.J. Kolata, R.J. Smith, K. Lamkin, R.E. Warner, Phys. Rev. Lett. **66**, 2452 (1991)
10. J.J. Kolata, A. Morsad, X.J. Kong, R.E. Warner, F.D. Becchetti, W.Z. Liu, D.A. Roberts, J.W. Jänecke, Nucl. Instrum. Methods B **40**, 503 (1989)
11. F.D. Becchetti, W.Z. Liu, D.A. Roberts, , J.W. Jänecke, J.J. Kolata, A. Morsad, X.J. Kong, R.E. Warner, Phys. Rev. C **40**, R1104 (1989)
12. M. Oshima, Y. Gono, T. Murakami, H. Kusakari, M. Sugawara, S. Ichikawa, Y. Hatsukawa, T. Morikawa, B.J. Min, Nucl. Instrum. Methods A **312**, 425 (1992)
13. D.C. Radford, C. Baktash, J.R. Beene, B. Fuentes, A. Galindo-Uribarri, C.J. Gross, P.A. Hausladen, T.A. Lewis, P.E. Mueller, E. Padilla, D. Shapira, D.W. Stracener, C.H. Yu, C.J. Barton, M.A. Caprio, L. Coraggio, A. Covello, A. Gargano, D.J. Hartley, N.V. Zamfir, Phys. Rev. Lett. **88**(22), 222501 (2002)
14. J.R. Beene, R.L. Varner, C. Baktash, A. Galindo-Uribarri, C.J. Gross, J.G. del Campo, M.L. Halbert, P.A. Hausladen, Y. Larochelle, J.F. Liang, J. Mas, P.E. Mueller, E. Padilla-Rodal, D.C. Radford, D. Shapira, D.W. Stracener, J.P. Urrego-Blanco, C.H. Yu, Nuclear Phys. A **746**, 471C (2004)
15. E. Padilla-Rodal, A. Galindo-Uribarri, C. Baktash, J.C. Batchelder, J.R. Beene, R. Bijker, B.A. Brown, O. Castanos, B. Fuentes, J.G. del Campo, P.A. Hausladen, Y. Larochelle, A.F. Lisetskiy, P.E. Mueller, D.C. Radford, D.W. Stracener, J.P. Urrego, R.L. Varner, C.H. Yu, Phys. Rev. Lett. **94**, 122501 (2005)
16. O. Niedermaier, H. Scheit, V. Bildstein, H. Boie, J. Fitting, R. von Hahn, F. Kock, M. Lauer, U.K. Pal, H. Podlech, R. Repnow, D. Schwalm, C. Alvarez, F. Ames, G. Bollen, S. Emhofer, D. Habs, O. Kester, R. Lutter, K. Rudolph, M. Pasini, P.G. Thirolf, B.H. Wolf, J. Eberth, G. Gersch, H. Hess, P. Reiter, O. Thelen, N. Warr, D. Weisshaar, F. Aksouh, P.V. den Bergh, P.V. Duppen, M. Huyse, O. Ivanov, P. Mayet, J.V. de Walle, J. Aysto, P.A. Butler, J. Cederkall, P. Delahaye, H.O.U. Fynbo, L.M. Fraile, O. Forstner, S. Franchoo, U. Koster, T. Nilsson, M. Oinonen, T. Sieber, F. Wenander, M. Pantea, A. Richter, G. Schrieder, H. Simon, T. Behrens, R. Gernhauser, T. Kroll, R. Krucken, M. Munch, T. Davinson, J. Gerl, G. Huber, A. Hurst, J. Iwanicki, B. Jonson, P. Lieb, L. Liljeby, A. Schempp, A. Scherillo, P. Schmidt, G. Walter, Phys. Rev. Lett. **94**, 172501 (2005)
17. J. Cederkall, A. Ekstrom, C. Fahlander, A.M. Hurst, M. Hjorth-Jensen, F. Ames, A. Banu, P.A. Butler, T. Davinson, U.D. Pramanik, J. Eberth, S. Franchoo, G. Georgiev, M. Gorska, D. Habs, M. Huyse, O. Ivanov, J. Iwanicki, O. Kester, U. Koster, B.A. Marsh, O. Niedermaier, T. Nilsson, P. Reiter, H. Scheit, D. Schwalm, T. Sieber, G. Sletten, I. Stefanescu, J.V. de Walle, P.V. Duppen, N. Warr, D. Weisshaar, F. Wenander, Phys. Rev. Lett. **98**, 172501 (2007)
18. I. Stefanescu, G. Georgiev, F. Ames, J. Aysto, D.L. Balabanski, G. Bollen, P.A. Butler, J. Cederkall, N. Champault, T. Davinson, A.D. Maesschalck, P. Delahaye, J. Eberth, D. Fedorov, V.N. Fedosseev, L.M. Fraile, S. Franchoo, K. Gladnishki, D. Habs, K. Heyde, M. Huyse, O. Ivanov, J. Iwanicki, J. Jolie, B. Jonson, T. Kroll, R. Krucken, O. Kester, U. Koster, A. Lagoyannis, L. Liljeby, G.L. Bianco, B.A. Marsh, O. Niedermaier, T. Nilsson, M. Oinonen, G. Pascovici, P. Reiter, A. Saltarelli, H. Scheit, D. Schwalm, T. Sieber, N. Smirnova,

J.V.D. Walle, P.V. Duppen, S. Zemlyanoi, N. Warr, D. Weisshaar, F. Wenander, Phys. Rev. Lett. **98**, 122701 (2007)
19. A.M. Hurst, P.A. Butler, D.G. Jenkins, P. Delahaye, F. Wenander, F. Ames, C.J. Barton, T. Behrens, A. Burger, J. Cederkall, E. Clement, T. Czosnyka, T. Davinson, G. de Angelis, J. Eberth, A. Ekstrom, S. Franchoo, G. Georgiev, A. Gorgen, R.D. Herzberg, M. Huyse, O. Ivanov, J. Iwanicki, G.D. Jones, P. Kent, U. Koster, T. Kroll, R. Krucken, A.C. Larsen, M. Nespolo, M. Pantea, E.S. Paul, M. Petri, H. Scheit, T. Sieber, S. Siem, J.F. Smith, A. Steer, I. Stefanescu, N.U.H. Syed, J.V. de Walle, P.V. Duppen, R. Wadsworth, N. Warr, D. Weisshaar, M. Zielinska, Phys. Rev. Lett. **98**, 072501 (2007)
20. P.V. Duppen, The Euroschool Lectures on Physics with Exotic Beams, p. 37, (Springer 2006)
21. S. Wan, P. Reiter, J. Cub, H. Emling, J. Gerl, R. Schubart, D. Schwalm, Z. Phys. A **356**, 231 (1997)
22. M. Belleguic, M.J. Lopez-Jimenez, M. Stanoiu, F. Azaiez, M.G. Saint-Laurent, O. Sorlin, N.L. Achouri, J.C. Angelique, C. Bourgeois, C. Borcea, J.M. Daugas, C. Donzaud, F.D. Oliveira-Santos, J. Duprat, S. Grevy, D. Guillemaud-Mueller, S. Leenhardt, M. Lewitowicz, U.E. Penionzhkevich, Y. Sobolev, Nucl. Phys. A **682**, 136C (2001)
23. P.G. Hansen, J.A. Tostevin, Annu. Rev. Nucl. Part. Sci. **53**, 221 (2003)
24. D. Bazin, B.A. Brown, C.M. Campbell, J.A. Church, D.C. Dinca, J. Enders, A. Gade, T. Glasmacher, P.G. Hansen, W.F. Mueller, H. Olliver, B.C. Perry, B.M. Sherrill, J.R. Terry, J.A. Tostevin, Phys. Rev. Lett. **91**, 012501 (2003)
25. J.A. Tostevin, G. Podolyak, B.A. Brown, P.G. Hansen, Phys. Rev. C **70**, 064602 (2004)
26. J.A. Tostevin, B.A. Brown, Phys. Rev. C **74**, 064604 (2006)
27. S. Michimasa, S. Shimoura, H. Iwasaki, A. Tamaki, S. Ota, N. Aoi, H. Baba, N. Iwasa, S. Kanno, S. Kubono, K. Kurita, A. Kurokawa, T. Minemura, T. Motobayashi, M. Notani, H.J. Ong, A. Saito, H. Sakurai, E. Takeshita, S. Takeuchi, Y. Yanagisawa, A. Yoshida, Phys. Lett. B **638**, 146 (2006)
28. A. Winther, K. Alder, Nucl. Phys. A **319**, 518 (1979)
29. T. Glasmacher, Annu. Rev. Nucl. Part. Sci. **48**, 1 (1998)
30. T. Suomijärvi, D. Beaumel, Y. Blumenfeld, P. Chomaz, N. Frascaria, J.P. Garron, J.C. Roynette, J.A. Scarpaci, J. Barrette, B. Fernandez, J. Gastebois, Nucl. Phys. A **509**, 369 (1990)
31. K.L. Yurkewicz, D. Bazin, B.A. Brown, C.M. Campbell, J.A. Church, D.C. Dinca, A. Gade, T. Glasmacher, M. Honma, T. Mizusaki, W.F. Mueller, H. Olliver, T. Otsuka, L.A. Riley, J.R. Terry, Phys. Rev. C **70**, 034301 (2004)
32. W.W. Wilcke, J.R. Birkelund, H.J. Wollersheim, A.D. Hoover, J.R. Huizenga, W.U. Schroeder, L.E. Tubbs, At. Data Nucl. Data Tables **25**, 391 (1980)
33. H. Olliver, T. Glasmacher, A.E. Stuchbery, Phys. Rev. C **68**, 044312 (2003)
34. D. Bazin, J.A. Caggiano, B.M. Sherrill, J. Yurkon, A. Zeller, Nucl. Instrum. Methods Phys. Res. B **204**, 629 (2003)
35. W.F. Mueller, J.A. Church, T. Glasmacher, D. Gutknecht, G. Hackman, P.G. Hansen, Z. Hu, K.L. Miller, P. Quirin, Nucl. Instrum. Methods Phys. Res. A **466**, 492 (2001)
36. T. Motobayashi, Y. Ikeda, Y. Ando, K. Ieki, M. Inoue, N. Iwasa, T. Kikuchi, M. Kurokawa, S. Moriya, S. Ogawa, H. Murakami, S. Shimoura, Y. Yanagisawa,

T. Nakamura, Y. Watanabe, M. Ishihara, T. Teranishi, H. Okuno, R.F. Casten, Phys. Lett. B **346**, 9 (1995)
37. L. Biederharn, P. Brussard, Coulomb Excitation, (Clarendon Press, Oxford, 1965)
38. P. Morse, H. Feshbach, Methods of theoretical physics, (McGraw-Hill, New York, 1953)
39. C.F. Weizsäcker, Z. Physics **88**, 612 (1934)
40. E.J. Williams, Phys. Rev. **45**, 729 (1934)
41. E. Fermi, Z. Phys. **29**, 315 (1924)
42. B. Hoffman, G. Baur, Phys. Rev. C **30**, 247 (1984)
43. A. Goldberg, Nucl. Phys. A **240**, 636 (1984)
44. C.A. Bertulani, G. Baur, Nucl. Phys. A **442**, 739 (1985)
45. C.A. Bertulani, G. Baur, Phys. Rep. **163**, 299 (1988)
46. C. Bertulani, A. Nathan, Nucl. Phys. A **554**, 158 (1993)
47. C. Bertulani, C. Campbell, T. Glasmacher, Comp. Phys. Comm. **152**, 317 (2003)
48. A.N.F. Aleixo, C.A. Bertulani, Nucl. Phys. A **505**, 448 (1989)
49. C.A. Bertulani, A. Stuchberry, T. Mertzimekis, A. Davies, Phys. Rev. C **68**, 044609 (2003)
50. D.J. Millener, J.W. Olness, E.K. Warburton, S. Hanna, Phys. Rev. C **28**, 497 (1983)
51. R. Anne, D. Bazin, R. Bimbot, M.J.G. Borge, J.M. Corre, S. Dogny, H. Emling, D. Guillemaud-Mueller, P.G. Hansen, P. Hornshøj, P. Jensen, B. Jonson, M. Lewitowicz, A.C. Mueller, R. Neugart, T. Nilsson, G. Nyman, F. Pougheon, M.G. Saint-Laurent, G. Schrieder, O. Sorlin, O. Tengblad, K. Wilhelmsen-Rolander, Z. Phys. A **352**, 397 (1995)
52. N. Summers, S. Pain, N. Orr, W. Catford, J. Angélique, N. Ashwood, N.C. V. Bouchat, N.M. Clarke, M. Freer, B. Fulton, F. Hanappe, M. Labiche, J. Lecouey, R. Lemmon, D. Mahboub, A. Ninane, G. Normand, F. Nunes, N. Soic, L. Stuttge, C. Timis, I. Thompson, J. Winfield, V. Ziman, Phys. Lett. B **650**, 124 (2007)
53. T. Nakamura, T. Motobayashi, Y. Ando, A. Mengoni, T. Nishio, H. Sakurai, S. Shimoura, T. Teranishi, Y. Yanagisawa, M. Ishihara, Phys. Lett. B **394**, 11 (1997)
54. M.C.M. Fauerbach, T. Glasmacher, P. Hansen, R. Ibbotson, D. Morrissey, H. Scheit, P. Thirolf, M. Thoennessen, Phys. Rev. C **56**, 1(R) (1997)
55. S. Typel, G. Baur, Phys. Lett. B **356**, 186 (1995)
56. C.A. Bertulani, L.F. Canto, M.S. Hussein, Phys. Lett. B **353**, 413 (1995)
57. T. Tarutina, L.C. Chamon, M.S. Hussein, Phys. Rev. C **67**, 044605 (2003)
58. M. Husseein, R.L. ad F.M. Nunes, I. Thompson, Phys. Lett. B **640**, 91 (2006)
59. C. Thibault, R. Klapisch, C. Rigaud, A.M. Poskanzer, R. Prieels, L. Lessard, W. Reisdorf, Phys. Rev. C **12**, 644 (1975)
60. X. Campi, H. Flocard, A.K. Kerman, S. Koonin, Nucl. Phys. A **251**, 193 (1975)
61. E.K. Warburton, J.A. Becker, B.A. Brown, Phys. Rev. C **41**, 1147 (1990)
62. B.V. Pritychenko, T. Glasmacher, P.D. Cottle, M. Fauerbach, R.W. Ibbotson, K.W. Kemper, V. Maddalena, A. Navin, R. Ronningen, A. Sakharuk, H. Scheit, V.G. Zelevinsky, Phys. Lett. B **467**, 309 (1999)
63. J.A. Church, C.M. Campbell, D.C. Dinca, J. Enders, A. Gade, T. Glasmacher, Z. Hu, R.V.F. Janssens, W.F. Mueller, H. Olliver, B.C. Perry, L.A. Riley, K.L. Yurkewicz, Phys. Rev. C **72**, 054320 (2005)

64. H. Iwasaki, T. Motobayashi, H. Sakurai, K. Yoneda, T. Gomi, N. Aoi, N. Fukuda, Z. Fulop, U. Futakami, Z. Gacsi, Y. Higurashi, N. Imai, N. Iwasa, T. Kubo, M. Kunibu, M. Kurokawa, Z. Liu, T. Minemura, A. Saito, M. Serata, S. Shimoura, S. Takeuchi, Y. Watanabe, K. Yamada, Y. Yanagisawa, M. Ishihara, Phys. Lett. B **522**, 227 (2001)
65. G. Klotz, Phys. Rev. C **47**, 2502 (1993)
66. V. Chiste, A. Gillibert, A. Lepine-Szily, N. Alamanos, F. Auger, J. Barrette, F. Braga, M.D. Cortina-Gil, Z. Dlouhy, V. Lapoux, M. Lewitowicz, R. Lichtenthaler, R.L. Neto, S.M. Lukyanov, M. MacCormick, F. Marie, W. Mittig, N.A. Orr, F.D. Santos, A.N. Ostrowski, S. Ottini, A. Pakou, Y.E. Penionzhkevich, P. Roussel-Chomaz, J.L. Sida, Phys. Lett. B **514**, 233 (2001)
67. R.W. Ibbotson, T. Glasmacher, B.A. Brown, L. Chen, M.J. Chromik, P.D. Cottle, M. Fauerbach, K.W. Kemper, D.J. Morrissey, H. Scheit, M. Thoennessen, Phys. Rev. Lett. **80**, 2081 (1998)
68. B.V. Pritychenko, T. Glasmacher, P.D. Cottle, M. Fauerbach, R.W. Ibbotson, K.W. Kemper, V. Maddalena, A. Navin, R. Ronningen, A. Sakharuk, H. Scheit, V.G. Zelevinsky, Phys. Lett. B **461**, 322 (1999)
69. P.D. Cottle, M. Fauerbach, T. Glasmacher, R.W. Ibbotson, K.W. Kemper, B. Pritychenko, H. Scheit, M. Steiner, Phys. Rev. C **60**, 031301 (1999)
70. P.D. Cottle, V.B. Pritychenko, J.A. Church, M. Fauerbach, T. Glasmacher, R.W. Ibbotson, K.W. Kemper, H. Scheit, M. Steiner, Phys. Rev. C **64**, 057304 (2001)
71. P.D. Cottle, Z. Hu, B.V. Pritychenko, J.A. Church, M. Fauerbach, T. Glasmacher, R.W. Ibbotson, K.W. Kemper, L.A. Riley, H. Scheit, M. Steiner, Phys. Rev. Lett. **88**, 172502 (2002)
72. A. Gade, D. Bazin, A. Becerril, C.M. Campbell, J.M. Cook, D.J. Dean, D.C. Dinca, T. Glasmacher, G.W. Hitt, M.E. Howard, W.F. Mueller, H. Olliver, J.R. Terry, K. Yoneda, Phys. Rev. Lett. **95**, 022502 (2005)
73. K.L. Yurkewicz, D. Bazin, B.A. Brown, C.M. Campbell, J.A. Church, D.C. Dinca, A. Gade, T. Glasmacher, A. Honma, T. Mizusaki, W.F. Mueller, H. Olliver, T. Otsuka, L.A. Riley, J.R. Terry, Phys. Rev. C **70**, 054319 (2004)
74. D.C. Dinca, R.V.F. Janssens, A. Gade, D. Bazin, R. Broda, B.A. Brown, C.M. Campbell, M.P. Carpenter, P. Chowdhury, J.M. Cook, A.N. Deacon, B. Fornal, S.J. Freeman, T. Glasmacher, M. Honma, F.G. Kondev, J.L. Lecouey, S.N. Liddick, P.F. Mantica, W.F. Mueller, H. Olliver, T. Otsuka, J.R. Terry, B.A. Tomlin, K. Yoneda, Phys. Rev. C **71**, 041302 (2005)
75. S. Raman, At. Data Nucl. Data Tables **78**, 1 (2001)
76. J.M. Cook, T. Glasmacher, A. Gade, Phys. Rev. C **73**, 024315 (2006)
77. B.V. Pritychenko et al, Phys. Rev. C **63**, 011305(R) (2001)
78. B. Perry, C. Campbell, J. Church, D. Dinca, J. Enders, T. Glasmacher, Z. Hu, K. Miller, W. Mueller, H. Olliver, Nucl. Instr. Meth. A **505**(1-2), 85 (2003)
79. N. Kaloskamis, K. Chan, A. Chishti, J. Greenberg, C. Lister, S. Freedman, M. Wolanski, J. Last, B. Utts, Nucl. Instr. Meth. A **330**, 447 (1993)
80. H. Wollersheim, D. Appelbe, A. Banu, R. Bassini, T. Beck, F. Becker, P. Bednarczyk, K.H. Behr, M. Bentley, G. Benzoni, C. Boiano, U. Bonnes, A. Bracco, S. Brambilla, A. Brunle, A. Burger, K. Burkard, P. Butler, F. Camera, D. Curien, J. Devin, P. Doornenbal, C. Fahlander, K. Fayz, H. Geissel, J. Gerl, M. Gorska, H. Grawe, J. Grebosz, R. Griffiths, G. Hammond, M. Hellstrom, J. Hoffmann, H. Hubel, J. Jolie, J. Kalben, M. Kmiecik, I. Kojouharov,

R. Kulessa, N. Kurz, I. Lazarus, J. Li, J. Leske, R. Lozeva, A. Maj, S. Mandal, W. Meczynski, B. Million, G. Munzenberg, S. Muralithar, M. Mutterer, P. Nolan, G. Neyens, J. Nyberg, W. Prokopowicz, V. Pucknell, P. Reiter, D. Rudolph, N. Saito, T. Saito, D. Seddon, H. Schaffner, J. Simpson, K.H. Speidel, J. Styczen, K. Sümmerer, N. Warr, H. Weick, C. Wheldon, O. Wieland, M. Winkler, M. Zieblinski, Nucl. Instrum. Methods Phys. Res. A **537**, 637 (2005)

81. S. Shimoura, Nucl. Instr. Methods A **525**, 188 (2004)
82. M.A. Deleplanque, I. Lee, K. Vetter, G.J. Schmid, F.S. Stephens, R.M. Clark, R.M. Diamond, P. Fallon, A.O. Macchiavelli, Nucl. Instrum. Methods A **430** (1999)
83. J. Gerl, Acta Phys. Polonica B **34**, 2481 (2003)
84. J. Simpson, J. Phys. G. **31**, S1801 (2005)